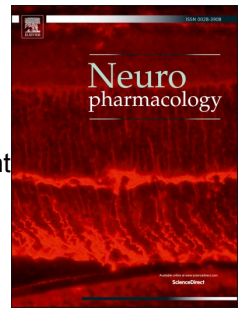

Malfunction of astrocyte and cholinergic inputs is involved in postoperative impairment of hippocampal synaptic plasticity and cognitive function

Tianhai Wang, Guiping Xu, Xue Zhang, Yanghao Ren, Tianyu Yang, Cheng Xiao, Chunyi Zhou

PII: S0028-3908(22)00250-7

DOI: https://doi.org/10.1016/j.neuropharm.2022.109191

Reference: NP 109191

To appear in: *Neuropharmacology*

Received Date: 28 January 2022

Revised Date: 4 June 2022

Accepted Date: 7 July 2022

Please cite this article as: Wang, T., Xu, G., Zhang, X., Ren, Y., Yang, T., Xiao, C., Zhou, C., Malfunction of astrocyte and cholinergic inputs is involved in postoperative impairment of hippocampal synaptic plasticity and cognitive function, *Neuropharmacology* (2022), doi: https://doi.org/10.1016/j.neuropharm.2022.109191.

Author contribution

C.Z. and G.X. designed the experiments and supervised the study. T.W. and X.Z. performed mouse surgery. T.W., X.Z., Y.R., and T.Y. collected and analyzed image and behavioral data. C.X. and C.Z. acquired and analyzed all electrophysiological data. T.W., G.X., C.X., and C.Z. wrote the manuscript. Every author read and approved the manuscript.

Malfunction of astrocyte and cholinergic inputs is involved in postoperative impairment of hippocampal synaptic plasticity and cognitive function

Tianhai Wang[1], Guiping Xu[3*], Xue Zhang[2], Yanghao Ren[4], Tianyu Yang[4], Cheng Xiao[2], Chunyi Zhou[2*]

1 Department of Anesthesiology, the Third Hospital, affiliated to Xinjiang Medical University, Urumqi, Xinjiang, China

2 Jiangsu Province Key laboratory in Anesthesiology, School of Anesthesiology, Xuzhou Medical University, Xuzhou, Jiangsu, China

3 Department of Anesthesiology, People's Hospital of Xinjiang Uygur Autonomous Region, Urumqi, Xinjiang, China

4 Graduate School of Xinjiang Medical University, Urumqi, Xinjiang, China

* Corresponding author:

Guiping Xu, MD, PhD

Email: xgpsyl@126.com

Chunyi Zhou, MD, PhD

Email: chunyi.zhou@xzhmu.edu.cn

Abstract

Postoperative delirium (POD) occurs in a few days after major surgery under general anesthesia and may cause serious health problems. However, effective intervention and treatment remain unavailable because the underlying mechanisms have far been elucidated. In the present study, we explored the role of the malfunctioned astrocytes in POD. Our results showed that mice with tibia fracture displayed spatial and temporal memory impairments, reduced LTP, and activated astrocytes in the hippocampus in early postoperative stage. Using electrophysiological and Ca^{2+} imaging techniques in hippocampal slices, we demonstrated the malfunctions of astrocytes in surgery mice: depolarized resting membrane potential, higher membrane conductance and capacitance, and attenuated Ca^{2+} elevation in response to external stimulation. The degraded calcium signaling in hippocampal astrocytes in surgery mice was restored by correcting the diminution of acetylcholine release with galantamine. Furthermore, pharmacologically blocking astrocyte activation with fluorocitrate and enhancing cholinergic inputs with galantamine normalized hippocampal LTP in surgery mice. Finally, inhibition of astrocyte activation with fluorocitrate in the hippocampus improved cognitive function in surgery mice. Therefore, the prevention of astrocyte activation may be a valuable strategy for the intervention of cognitive dysfunction in POD, and acetylcholine receptors may be valid drug targets for this purpose.

Keywords: Postoperative delirium; Hippocampus; Astrocytes; Cholinergic inputs; Synaptic plasticity; Cognitive function

1. Introduction

Postoperative delirium (POD) occurs between 2–5 postoperative days. It is a subject of great interest since the incidence of POD reaches 50–70% in patients undergoing major surgeries or suffering from mental problems (Inouye et al., 2014; Saczynski et al., 2012; Wilson et al., 2020), and POD is a risk factor of long-term cognitive impairment (Moskowitz et al., 2017; Pandharipande et al., 2013; Saczynski et al., 2012). However, the mechanisms underlying POD have far been elucidated.

Growing evidence suggests that neuroinflammation is implicated in POD (Lin et al., 2020; Safavynia and Goldstein, 2018). The peripheral inflammation leads to the structural and functional damages in the blood brain barrier, through which inflammatory cells and mediators translocate into the central nervous system and activate microglia and astrocytes (Li et al., 2020; Skvarc et al., 2018; Terrando et al., 2011). Astrocytes are well known to shape synapse formation and to modulate synaptic transmission and plasticity (Allen and Eroglu, 2017). In this regard, astrocytes may be responsible for the acute changes in synaptic plasticity in POD. However, little has been known about the pathophysiology of astrocytes in POD. Furthermore, it remains unclear whether activated astrocytes affect synaptic plasticity and contribute to the pathogenesis of POD.

Cholinergic system plays an important role in learning and memory (Haam and Yakel, 2017; Solari and Hangya, 2018). In particular, cholinergic neurons in the medial septum and diagonal band of Broca provide major cholinergic inputs to the hippocampus and have a great impact on hippocampal circuits and memory formation (Araque et al., 2002; Navarrete et al., 2012; Pabst et al., 2016). Recent studies demonstrated that cardiac and non-cardiac surgery patients with POD exhibit a lower level of acetylcholinesterase (Adam et al., 2020; Zhao et al., 2019). Our previous study showed that cholinergic activity was impaired in the hippocampus as increasing acetylcholine concentration with galantamine reversed cognitive dysfunction in mice subjected to tibial fracture (Wang et al., 2019). Hippocampal astrocytes express both nicotinic and muscarinic cholinergic receptors (Hernandez-Morales and Garcia-Colunga, 2009; Takata et al., 2011) and respond to locally released acetylcholine with an increase in Ca^{2+} concentration (Takata et al., 2011). These processes may contribute to cholinergic modulation of synaptic transmission, and learning and memory

(Navarrete et al., 2012; Pabst et al., 2016). These raise the possibility that the interaction between astrocytes and cholinergic inputs may participate in early cognitive dysfunction following peripheral surgery.

A mouse model with tibial fracture exhibits some of the cognitive impairments commonly observed in patients subjected to orthopedic surgery, and has been used to study mechanisms of postoperative neuroinflammation and behavioral changes (Hirsch et al., 2016; Terrando et al., 2011; Wang et al., 2019; Xiong et al., 2018). To shed light on the relationship between astrocytes and cognitive impairment in POD, we characterized modifications of hippocampal astrocytes, and measured acetylcholine release and synaptic plasticity in the hippocampus on postoperative day 3 in mice subjected to tibial fracture. With multidisciplinary experiments, we provide two intervention strategies (enhancing cholinergic function and inhibiting astrocyte activation) to effectively improve deficits in synaptic plasticity in the hippocampus and cognitive function in POD mice.

2. Materials and methods

2.1. Animals

The care and use of animals and the experimental protocols utilized in this study were approved by the Institutional Animal Care and Use Committee and the Office of Laboratory Animal Resources of Xinjiang Medical University and Xuzhou Medical University under the Regulations for the Administration of Affairs Concerning Experimental Animals (1988) in China. We used male C57/BL6 wild-type mice (5–7 month old) because there is no sex differences in the development of post-operative cognitive dysfunction in young adults (Schenning et al., 2019). Mice were group housed ($\leqslant$ 4) in a standard 12 h light / dark cycle with free access to food and water. All behavioral experiments were performed in the light cycle. Efforts were made to minimize animal suffering and to reduce the number of mice used.

2.2. Tibial fracture Surgery

A unilateral stabilized tibial fracture operation with intramedullary pinning was performed as described previously (Terrando et al., 2013; Wang et al., 2019). Mice were anesthetized with sodium pentobarbital (40 mg/kg). Briefly, the left hind limb was shaved and disinfected. A 0.5 cm longitudinal incision was made. Muscles were detached to expose the tibia and the periosteum was stripped. A 5 mm long stainless-steel pin (0.38 mm in diameter) was inserted into the tibia intramedullary canal and the hole was sealed with bone vax. Then, the skin was sutured. The mice were allowed to recover on a heating pad until woke up before returning to a clean home cage. For postoperative pain relief, ibuprofen (50 mg/L) was provided in drinking water *ad libitum*. Sham mice received anesthesia and analgesia without any surgical operation.

2.3. Contextual fear conditioning

Fear conditioning is a useful behavioral paradigm for assessing learning and memory (Wang et al., 2019). Contextual fear-conditioning was conducted as reported previously (Johansen et al., 2011; Shi et al., 2016; Wang et al., 2019). The test includes training (conditioning) and test sessions (Fig. 1A). Before each training and test session, mice were brought to the testing room and allowed to habituate for at least 60 min. Mice were handled daily for 5 days prior to training. In the training session, mice were first

placed in the fear-conditioning chamber (Med Associates, Fairfax, VT) and allowed to explore for 120 s; a tone (70 dB) (conditional stimulus, CS) was then presented for 20 s and a constant mild foot shock (0.8 mA) (unconditional stimulus, US) was given at the last 2 s. Three trials of tone-foot shock pairings separated by 2 min intervals were delivered (Fig. 1A). The mice remained in training chamber for another 30 s before being returned to home cages. Test session was performed 3 days after the operation (Fig. 1A). Mice were placed into the same fear-conditioning chamber (the contextual cue) and allowed to free roaming for 2 min without a tone or a shock. Their movement in this period was monitored by a tracking system (Med Associates, Fairfax, VT). The percentage of the total time the mice spent freezing in the chamber and the index of the contextual memory were calculated by the software of the fear conditioning system (Med Associates, Fairfax, VT).

The chamber was wiped clean with 70% alcohol between mice.

2.4. Novel object recognition

The novel object recognition (NOR) test was used to evaluate cognitive function in mice, based on the phenomenon that rodents tend to spend longer time exploring a novel object than a familiar one (Leger et al., 2013). In the familiarization session, the mice were allowed to explore two identical objects 15 cm apart for 10 min in an open field arena (40 × 40 × 40 cm). Five hours later, one object was replaced with a novel one, and the mice were placed in the open field arena again to explore the familiar and novel objects for 10 min. The time spent exploring each object was recorded. Novel object discrimination index was calculated as the ratio of the time the mouse spent exploring novel object to the total time the mouse spent exploring the familiar and novel objects in the test session. The total distance traveled and the average velocity during the test session were compared between the two groups to rule out the interference of object exploration by altered motor function. The video data were analyzed with a movement tracking system, Ethovision XT 14.0 (Noldus Information Technology, Wageningen, The Netherlands)

2.5. Measurement of acetylcholine release with an ACh sensor

Individual mice were anesthetized by intraperitoneal injection of sodium pentobartital (40 mg/kg). The head of the mouse was stabilized on a stereotaxic frame

(RWD Life Science Co., Ltd, Shenzhen, China) while its body was placed on a heating pad. The surgery was performed as described previously (Luan et al., 2020). Viral vector carrying ACh sensor (AAV-hSyn-GACh3.0, $3x10^{12}$ vg/ml, WZ Biosciences Inc., Jinan, China) (150 nl) was injected at the speed of 50 nl/min into the dorsal hippocampus with a microsyringe pump (WPI Inc., Sarasota, FL). The coordinate of the hippocampus is: −1.90 mm from the Bregma at anterior to posterior axis; 1.80 mm deep from the Bregma; ±1.25 mm from the midline. Three weeks later, acute hippocampal slices (300 μm thick) were prepared for experiments.

GACh in the CA1 region of the hippocampus was imaged with an epi-fluorescent microscope (FN-1, Nikon, Tokyo, Japan). Sequence images were acquired (9 frames / s) with a CCD Camera (Flash LTE 4.0, Hamamatsu, Hamamatsu city, Japan) controlled by the HCImage 4.0 software (Hamamatsu, Hamamatsu city, Japan), which was also used for analysis of imaging data.

2.6. Hippocampal slice preparation

The mice were deeply euthanized with CO_2, and then intracardiac perfusion was performed with ice-cold modified sucrose-based artificial cerebral spinal fluid (sACSF, 5 ml/min) saturated with 95% O_2 / 5% CO_2 (carbogen) containing (mM): 85 NaCl, 75 sucrose, 2.5 KCl, 1.25 NaH_2PO_4, 4.0 $MgCl_2$, 0.5 $CaCl_2$, 24 $NaHCO_3$ and 25 glucose (Luan et al., 2020; Tang et al., 2021; Wang et al., 2019). The brain was rapidly removed and placed in ice-cold sACSF. 300 μm thick coronal hippocampal slices, prepared with a Leica VT-1200S vibratome (Wetzlar, Germany), were incubated in carbogenated sACSF at 32 ± 1 ℃ in a holding chamber for an hour. The slices were then transferred into normal ACSF, containing (mM): 125 NaCl, 2.5 KCl, 1.2 NaH_2PO_4, 1.2 $MgCl_2$, 2.4 $CaCl_2$, 26 $NaHCO_3$, and 11 glucose, and were kept at room temperature for at least 30 min before used for both imaging and electrophysiological experiments.

A borosilicate glass with a 10 μm tip, fabricated with a horizontal pipette puller (P-1000, Sutter Instrument Inc., Novato, CA), was filled with ACSF, connected to a stimulus isolator (Iso-Flex, AMPI, Jerusalem, Israel), and placed in the stratum oriens / alveus area (O/A), where the septohippocampal cholinergic terminals locate (Araque et al., 2002; Navarrete et al., 2012).

2.7. Sulforhodamine 101 (SR101) loading

Hippocampal slices were stained with a red fluorescent astrocyte marker, sulforhodamine 101 (SR101, 5 μM), in carbogenated ACSF for 35 min at 34 ℃ (Boddum et al., 2016) and were subsequently returned to dye-free ACSF for at least 30 min before imaging.

2.8. Calcium imaging in astrocytes

Calcium levels in astrocytes of the hippocampal CA1 region were monitored using a calcium indicator, Fluo-4 AM (a green fluorophore), as reported previously (Cameron et al., 2016; Reeves et al., 2011). Fluo-4 AM was dissolved in DMSO containing 1% pluronic acid-127 into the final concentration of 1 mM and sonicated for 15 min. Brain slices were incubated with 5 μM Fluo-4 AM and 5 μM SR101 in ACSF oxygenated continuously with 95% O_2-5% CO_2 at 34 ℃ in the dark for 45 min. The slices were then transferred to dye-free ACSF for at least 30 min before imaging.

A hippocampal slice was placed in a recording chamber, perfused with carbogenated ACSF at 32 ℃. SR101-labeled astrocytes were visualized with red fluorescent illumination and Fluo-4-labeled astrocytes were imaged with green fluorescent illumination under a microscope (FN-1, Nikon, Tokyo, Japan) equipped with a 40× water immersion objective (NA = 0.80, WD = 3.5 mm). Time sequence images (9 frames/s) of Fluo-4 were acquired with a CMOS-CCD camera (Flash 4.0 LTE, Hamamatsu, Hamamatsu city, Japan) controlled by the HCImage 4.0 software (Hamamatsu, Hamamatsu city, Japan). The fluorescence intensity of Fluo-4 signal from each astrocyte was plotted versus time. Subsequent electrical stimulation (0.1 ms, 20 Hz, for 1 s)-evoked changes in fluorescence intensity (ΔF) in each trial was normalized to the average fluorescence intensity before electrical stimulation ($\Delta F/F_0$). Astrocytes were considered responsive to electrical stimulation when $\Delta F/F_0$ increased more than two times of the standard deviation of F_0.

2.9. Electrophysiological recordings in hippocampal astrocytes

Slices were transferred into a chamber, superfused with carbogen saturated ACSF (2 ml/min, 32 ± 1 ℃). Whole-cell patch-clamp signals were recorded from SR101-stained astrocytes in the CA1 region of the hippocampus with a MultiClamp 700B amplifier, a Digidata 1552B analog-to-digital (AD) converter, and the pClamp 10.7

software (Molecular Devices, San Jose, CA). The patch electrode had a resistance of 5 – 8 MΩ when filled with an intrapipette solution containing (in mM) 135 K gluconate, 5 KCl, 0.2 EGTA, 0.5 $CaCl_2$, 10 HEPES, 2 Mg-ATP, and 0.1 GTP (pH was adjusted to 7.2 with Tris-base; osmolarity was adjusted to 300 mOsm with sucrose). The junction potential between patch pipette and bath solutions was nulled just before gigaseal formation. Series resistance was monitored without compensation throughout the experiment using the MultiClamp 700B commander (Molecular Devices, San Jose, CA). Data were sampled at 10 kHz and were filtered at 2 kHz.

2.10. Recordings of field excitatory postsynaptic potential

Field excitatory postsynaptic potentials (fEPSPs) were recorded with a MultiClamp 700B amplifier and a Digidata 1552B AD converter (Molecular Devices, San Jose, CA) in the current-clamp mode from the CA1 region of the hippocampus with a glass microelectrode (2–5 MOhm) (Popov et al., 2021). An ACSF-filled electrode was placed in the Schaffer collateral commissural pathway (SC) to deliver electrical stimulation (0.1 ms, 0.05 Hz, 20–200 μA) (Iso-Flex, AMPI, Jerusalem, Israel). The high frequency stimulation (HFS) used to induce LTP consists of 3 trains of 0.2 s 100 Hz pulses (0.1 ms) with 20 s intervals. Stimulation intensities were adjusted (20–40 μA) to evoke half-maximal responses. The HFS was applied only if the amplitudes of the fEPSPs were stable for at least 20 min. After HFS, the fEPSPs were recorded at least 60 min. The wide band signal was digitally low-pass filtered at 2 kHz. The LTP magnitude was calculated as % increase of the potentiated fEPSP amplitude relative to the baseline fEPSP amplitude.

2.11 Bilateral intracranial injection of fluorocitrate

Stainless steel guide cannulas (26G, RWD Life Science, Shenzhen, China) were bilaterally implanted 500 μm above the CA1 region in the dorsal hippocampus and were fixed to the skull with dental cement (Yuyan, Shanghai, China). The mice were allowed to recover for a week. For postoperative pain relief, ibuprofen (50 mg/L) was added in drinking water for 3 days. A 30-gauge injection needle (500 μm longer than the cannula) was inserted in the dorsal hippocampus through the cannula for the delivery of FC (400 nl/side, 50 nl/min) with a microsyringe pump (WPI, Sarasota, FL) while the mice were lightly anesthetized with an isoflurane evaporator (RWD Life Science Co., Ltd,

Shenzhen, China). By the end of the infusion, the injection needles remained inside the guide cannula for 5-10 min to insure adequate absorption of FC by the tissue. Locations of cannula implants in mice were confirmed histologically after the experiments.

2.12 Immunohistochemistry

Mice were sacrificed in a CO_2 chamber and subjected to transcardiac perfusion with phosphate-buffered saline (PBS) followed by 4% paraformaldehyde (PFA). The brains were removed and post-fixed in PFA for 4–6 h followed by gradient sucrose dehydration for two days at 4 ℃. After dehydration, brains were sectioned into 30 μm slices with a Leica CM1950 cryostat (Wetzlar, Germany) and the slices were mounted onto glass slides, which were kept at -20 ℃.

The frozen slices on the glass slides were washed twice (10 min each) with cold PBS, blocked for 1 h at room temperature in 0.1% Triton X-100 and 4% donkey serum in PBS, followed by incubation in a primary antibody (1:500, mouse anti-GFAP, Santa Cruz, Dallas, TX) in 0.1% Triton X-100 and 1% donkey serum in PBS at 4 °C for 24 h. After three washes (10 min each) with PBS, the slices were incubated with secondary antibody (1:500, donkey anti-mouse, Jackson ImmunoResearch, West Grove, PA) with PBS at room temperature for 2 h. The sections were washed three times (10 min each) with PBS, dried at room temperature, and cover-slipped in mounting medium.

The stained slices were imaged under 10× and 20× objectives with a Zeiss LSM 880 confocal microscope (Zeiss, Oberkochen, Germany). The images were processed with Image J (NIH, Bethesda, MD).

2.12 Drugs

Fluo-4-AM and SR101 were purchased from Thermo Fisher Scientific (Waltham, MA). DL-fluorocitric acid barium (FC) was from Sigma-Aldrich (Saint Louis, MO). All other drugs were from MedChemExpress (Monmouth Junction, NJ).

The FC solution was prepared as follows: 8 mg FC was dissolved in 1 mL 0.1 mol/L HCl. Two to three drops of 0.1 mol/L Na_2SO_4 were added to precipitate the Ba^{2+}. The suspension was diluted in 0.9% NaCl to the final concentration and the pH was adjusted to 7.4. For behavioral test, 1 nmol/μl FC (400 nl/side) was injected in the dorsal hippocampus. For brain slice recording, scopolamine (Scop, 5 μM), galantamine (Gal,

10 μM) or FC (100 μM) in ACSF was applied through bath perfusion.

2.13 Statistical analysis

GraphPad Prism 7.0 was used for all statistical analyses. All data were expressed as mean ± SEM. Two-tailed paired or unpaired t-test was used for comparison of parameters between two groups if the data passed the normality and equal variance tests. ANOVAs followed by post-hoc Bonferroni tests were used for multiple pair-wised comparisons. If the equal variance assumptions were not valid, statistical significance of the difference between groups was evaluated using the Mann–Whitney test or ANOVA rank tests. A value of $P < 0.05$ was considered statistically significant. The mean, SEM, n, the specific statistical test, F, t, and P values were reported in the figure legends.

3. Results

3.1 Impairment of cognitive function in surgery mice

To study the role of astrocytes in postoperative cognitive dysfunction, we first established a mouse model subjected to a major surgery under pentobarbital general anesthesia. We adopted an aseptic tibial fracture with internal fixation and anesthesia-matched sham procedure on mice. After recovery, we assessed cognitive function in the mice with two paradigms: aversive memory associated with a conditional stimulus (electric foot shock paired with a sound cue, fear conditioning) (Fig. 1A) and short-term visual and spatial memory (novel object recognition, NOR) (Fig. 1E).

In the fear-conditioning paradigm, sham and surgery mice displayed comparable exploring behavior in the apparatus in pre-conditioning session and freezing behavior during training session one day before the operation (Fig. 1B, 1C). In the contextual test session on post-operative day 3, surgery mice showed a significantly shorter freezing time in the training chamber (Fig. 1D). These data suggest that mice undergoing tibial fracture experienced hippocampus-dependent cognitive decline.

In NOR paradigm conducted on post-operative day 3, sham and surgery mice displayed comparable exploration time on the two identical objects (Fig. 1G) in the training session. During testing session, sham mice were able to discriminate between the familiar and novel objects as they spent a longer time in exploring the novel object than the familiar object (Fig. 1F, 1H). In contrast, surgery mice did not show a significant difference in time spent exploring the novel and familiar objects (Fig. 1F, 1H). Moreover, a lower discrimination index in NOR in surgery mice indicates worse performance than sham mice (Fig.1I). Note that there was no difference in total distance travelled or velocity between sham and surgery mice during the testing session (20 min distance: 27.9 $\pm$ 1.9 m and 22.3 $\pm$ 3.0 m in sham and surgery mice, respectively, $t = 1.56$, $P = 0.14$; Velocity: 4.7 $\pm$ 0.3 cm/s and 3.7 $\pm$ 0.5 cm/s in sham and surgery mice, respectively, $t = 1.54$, $P = 0.14$; 10 sham mice, 11 surgery mice), indicating that motor function is not affected by surgery.

These results confirm the validity of mice subjected to tibial fracture with internal fixation as a model to study cellular mechanisms underlying cognitive dysfunction in postoperative delirium (POD).

3.2 Surgery leads to activation and biophysical modifications in hippocampal

astrocytes

It has been revealed that astrocytes in the hippocampus respond to peripheral surgery with hypertrophy and hyperplasia (Li et al., 2020; Zhang et al., 2016). To verify whether astrocyte activation occurs after surgery, we counted the number of anti-GFAP antibody-stained astrocytes in the hippocampal CA1 region (Fig. 2A). The number of GFAP- positive cells (Fig. 2B) and the GFAP immunoreactive area in the hippocampal CA1 region significantly increased on post-operative day 3 (Fig. 2C). These data indicate that the surgery leads to astrogliosis.

Morphological remodeling affects various aspects of the physiology of astrocytes (Diaz-Castro et al., 2021; Popov et al., 2020). To understand whether CA1 astrocytes exhibit different biophysical properties between sham and surgery mice, we performed whole-cell patch-clamp recordings from live hippocampal slices prepared 2–3 days after surgery and sham operation.

The astrocytes were visualized by sulforhodamine 101 (SR101) staining and identified by their morphology (small and round cell bodies) (Fig. 2D). First, we obtained current–voltage relationships (I-V curves) of astrocytes by applying voltage steps to voltage-clamped astrocytes (V_H = -80 mV) (Fig. 2E). The linear relationship of I-V curves in astrocytes from sham and surgery groups indicates the passive membrane property of the astrocyte. However, the slope of the I-V curve in surgery mice increased relative to that in sham mice (Fig. 2F), indicating an increase in cell conductance (Fig. 2G). We also found that astrocytes in surgery mice had a more depolarized resting membrane potential than those in sham mice (Fig. 2H). Consistent with the notion that an activated astrocyte has an enlarged cell body, we observed that astrocytes in surgery mice displayed higher capacitance than those from sham mice (Fig. 2I).

These results suggest that surgery causes the activation of hippocampal astrocytes with modified biophysical properties.

3.3 Surgery impairs muscarinic receptor activation-evoked Ca^{2+} influx in hippocampal astrocytes

As Ca^{2+} influx is crucial for physiological function of astrocytes (Allen and Eroglu, 2017), we examined whether surgery affects Ca^{2+} elevation induced by electrical stimulation on post-operative day 3. Loading a calcium indicator Fluo-4 AM in cells in hippocampal slices allows real-time imaging of intracellular Ca^{2+}, meanwhile, SR101

enables labeling of astrocytes (Fig. 3A). With these two procedures, we were able to monitor Ca^{2+} concentration in astrocytes in response to electrical stimulation (Fig. 3B). We observed that electrical stimulation in the stratum oriens / alveus (O/A) of the hippocampal CA1 region caused Ca^{2+} elevation (Fig. 3C, 3D) in about 50% of astrocytes from sham and surgery mice (Fig. 3E), but with a larger amplitude in sham mice (Fig. 3F).

It is well-established that astrocytes express a repertoire of receptors for multiple neurotransmitters, including glutamate, GABA, ACh, and ATP (Ota et al., 2013). Given that the strong cholinergic afferents from the medial septum and the diagonal band of Broca are located in the O/A area of the hippocampus and CA1 astrocytes respond to cholinergic activation by increasing Ca^{2+} mobilization (Araque et al., 2002), we examined whether inhibition of muscarinic receptors attenuates electrical stimulation-evoked Ca^{2+} elevation in hippocampal astrocytes. We found that electrical stimulation of O/A area-evoked Ca^{2+} elevation was reliably inhibited by application of a non-selective muscarinic receptor antagonist, scopolamine (Scop, 5 μM), by 73.75% ± 7.07% (n = 10) and 76.25 ± 3.85% (n = 11) in sham and surgery mice, respectively (Fig. 3G - J). These data suggest that muscarinic receptor activation plays a pivotal role in mediating electrical stimulation-evoked Ca^{2+} elevation in astrocytes, similar to a previous report (Araque et al., 2002). We then subtracted electrical stimulation-evoked Fluo-4 signals in the presence of Scop from that in the absence of Scop and obtained a Scop-sensitive component (Fig. 3K). The comparison between the peak of stimulation-evoked Ca^{2+} elevation in astrocytes between sham and surgery mice reveals a significant impairment in muscarinic receptor function in hippocampal astrocytes in surgery mice (Fig. 3L).

These results demonstrated that muscarinic receptors mainly mediate the regulation of astrocytes by cholinergic inputs in the hippocampus, and this connection is impaired in surgery mice.

3.4 ACh release in the hippocampal CA1 region is reduced in surgery mice

To test whether cholinergic activity in the hippocampus is altered in surgery mice, we used a rapid, intensity-based ACh-sensing green fluorescent reporter (GACh) (Jing et al., 2020; Jing et al., 2018) to visualize the spatiotemporal dynamics of extracellular ACh in the hippocampus. We injected an AAV vector carrying GACh controlled by the

synapsin promoter (AAV2/1-hsyn-GACh) into the dorsal hippocampus (Fig. 4A). Three weeks after GACh expression, acute hippocampal slices were prepared from sham and surgery mice on post-operative day 3. ACh release was evoked by placing a stimulating electrode in the O/A of the hippocampal CA1 region (Fig. 4A), and wide field GACh responses were imaged with a CCD camera under the green fluorescent illumination.

A detectable rapid response to a brief burst of 20 pulses of electrical stimulation (20 μA) at 20 Hz was readily observed in area adjacent to the stimulating electrode in sham and surgery mice (Fig. 4B). However, the responses in surgery mice were much smaller than those in sham mice (Fig. 4B-D). These data suggest that reduced acetylcholine release may be associated with the impairment of cholinergic modulation of hippocampal astrocytes.

3.5 Galantamine enhances electrical stimulation-evoked astrocytic Ca^{2+} elevations in surgery mice

Next we sought to test whether galantamine (Gal), a cholinesterase inhibitor and a positive allosteric modulator of nicotinic acetylcholine receptors (nAChRs) (Coyle and Kershaw, 2001), repairs astrocytic Ca^{2+} elevation evoked by electrical stimulation in the hippocampal slices from surgery mice on post-operative day 3. Gal (10 μM) was chosen based on our previous study (Wang et al., 2019). To achieve this goal, we performed calcium imaging as shown in Fig. 3. We monitored Ca^{2+} elevation in individual CA1 astrocytes upon electrical stimulation (Fig. 3A, 3B). In control experiments, Ca^{2+} elevation in CA1 astrocytes was reliably induced by electrical stimulation in the O/A area of the hippocampal CA1 region in both sham and surgery mice (Fig. 5A, 5C). In the presence of Gal, electrical stimulation-evoked Ca^{2+} elevation in astrocytes was monitored every 2 min. The data showed that 10 min perfusion of Gal enhanced Ca^{2+} elevation in response to electrical stimulation in both sham and surgery mice (Fig. 5A - D). Interestingly, the enhancement of Ca^{2+} elevation by Gal was significantly stronger in surgery mice than in sham mice (Fig. 5E).

The data suggest that Gal may restore the cholinergic impairment-induced dysfunction in astrocytic Ca^{2+} elevations in surgery mice.

3.6 Astrocyte activation parallels impaired synaptic plasticity in surgery mice

Calcium signaling in astrocytes plays an important role in facilitating bidirectional communication between neurons and astrocytes (Allen and Eroglu, 2017). The dysfunction of astrocytic Ca^{2+} signaling in surgery mice led us to hypothesize that astrocytes may contribute to deficit in synaptic plasticity. Therefore, we examined whether dysfunction in astrocyte in surgery mice is associated with the impaired long-term potentiation (LTP) in the hippocampus, a major cellular mechanism underlying learning and memory (Bliss and Collingridge, 1993; Cooke and Bliss, 2006).

We recorded fEPSPs in acute hippocampal slices from sham and surgery mice on post-operative day 3 by placing a recording electrode in CA1 area and a stimulating electrode in the Schaffer collaterals (SC) pathway (Fig. 6A). The LTP was induced with high-frequency burst stimulation (HFS, 0.2 s 100 Hz repeated 3 times with 20 s intervals) (Fig. 6B). The fEPSP amplitude was transformed into % baseline (pre-HFS) fEPSP amplitude (Fig. 6C). We observed that HFS caused an enhancement in fEPSPs, which lasted for more than an hour in hippocampal slices from both sham and surgery mice (Fig. 6C). These data indicate that under our recording condition, HFS induces LTP. As expected, HFS-induced LTP in hippocampal slices was significantly attenuated in surgery mice than in sham control mice (Fig. 6D). To discriminate whether a presynaptic mechanism is involved in the degraded LTP in surgery mice, we evoked fEPSPs with pairs of electrical stimuli (separated by 100 ms, stimulated once every 20 s) and calculated paired-pulse ratios (Fig. 6E). We found that HFS did not change paired-pulse ratio in both sham and surgery mice (Fig. 6F). These data suggest that surgery impairs LTP likely through postsynaptic mechanisms.

To examine whether astrocyte activation is involved in the impairment of hippocampal LTP, we pre-incubated hippocampal slices in fluorocitrate (FC, 100 μM) for at least 20 min and then added FC in ACSF for bath perfusion to block the activation of glial cells. We observed that FC enhanced HFS-induced LTP in both sham and surgery mice (Fig. 6G, 6J, 6H, 6I, 6K, 6L). Interestingly, it enhanced HFS-triggered LTP in surgery mice to a level close to that in sham mice without FC (Surgery with FC: 211.5 ± 8.5, n = 6; Sham without FC: 201.6 ± 13.1, n = 10; t = 0.54, P = 0.6, two-tailed t-test; Fig 6I and 6L). As dysfunction of astrocytic Ca^{2+} elevation was restored by application of Gal in surgery mice (Fig. 5), we also investigated the effect of Gal on hippocampal LTP from sham and surgery mice in another set of experiments. Gal (10

μM) was applied 5 min before HFS and included in the perfusion throughout the experiments. The LTP triggered by HFS in the SC pathway was enhanced in the presence of Gal in both sham and surgery mice (Fig. 6G - 6L). In addition, LTP enhancement with Gal treatment was similar to that with FC treatment in sham and surgery mice, respectively (Fig. 6I and 6L).

Overall, our *in vitro* hippocampal slice data demonstrate that surgery mice exhibit weaker LTP than sham controls, but either blockade of astrocyte activation or enhancement of cholinergic inputs is sufficient to restore normal synaptic plasticity.

3.7 FC facilitates learning and memory in surgery mice

Since FC facilitated hippocampal LTP in surgery mice (Fig. 6), next we explored whether FC improves cognitive deficits in surgery mice. We performed bilateral cannula implantation in the dorsal hippocampus (Fig. 7A, 7B). Unilateral tibial fracture was performed one week after cannula implantation. We divided surgery mice into two subgroups, respectively received intra-hippocampal injection of FC (0.4 nmol, 400 nl in each side) and the same volume of saline once daily after surgery. The dose of FC (⩽ 1nmol) was chosen according to previous studies (Hassel et al., 1992; Hennes et al., 2020). We observed that this procedure significantly reduced astrocyte activation in the hippocampal CA1 region (Fig. 7C, 7D). Fear conditioning was performed with the same paradigm as that shown in Fig. 1A. Before surgery, we confirmed that the mice in different groups were similarly active (Fig. 7E). As illustrated in Fig. 7F, 3 days' intra-hippocampal injection of FC improved contextual memory in surgery mice. NOR was performed as the same paradigm shown in Fig. 1E. Both groups of mice did not show preference to either of two identical objects in training session (Fig. 7G), but surgery mice with 3 days' intra-hippocampal injection of FC spent a longer time in exploring the novel object than the familiar object and exhibited a higher novel object discrimination index (Fig. 7H, 7I). In contrast, surgery mice with saline treatment showed similar exploration time around familiar object and novel object and displayed a lower novel object discrimination index (Fig. 7H-7J). Additionally, the effect of FC injection in the hippocampus on motor function was not significantly different from that of saline injection in the hippocampus in surgery mice. Specifically, total distance traveled and velocity of movement in the test session were comparable between the two groups (Distance: 35.2 ± 2.9 m and 27.8 ± 2.4 m in saline and FC groups, respectively,

t = 1.98, P = 0.07; Velocity: 5.9 ± 0.5 cm/s and 4.6 ± 0.5 cm/s in saline and FC mice, respectively, t = 1.96, P = 0.07; those data were from 8 saline injection mice and 7 FC injection mice). Therefore, the data suggest that inhibition of astrocyte activation may be a potential therapeutic strategy for the intervention of cognitive deficit in POD.

4. Discussion

Pathophysiology of postoperative cognitive dysfunction remain unclear. Accumulating evidence has revealed that various modifications in neurotransmitters, astrocytes, neurons, synaptic transmission, and synaptic plasticity in the central nervous system result from the combination of anesthesia and major surgeries (Lin et al., 2020; Safavynia and Goldstein, 2018). In the present study, we demonstrate the link among activation and malfunction of astrocytes, reduced acetylcholine release, and impaired synaptic plasticity and cognitive function in mice subjected to a major surgery under general anesthesia. Our results showed that mice with tibial fracture displayed cognitive impairments, reduced cholinergic inputs and LTP, the activation of hippocampal astrocytes in early post-operative stages. Using electrophysiological recordings and Ca^{2+} imaging in hippocampal slices, we observed malfunction in hippocampal astrocytes in surgery mice: depolarized resting membrane potential, higher membrane conductance and capacitance, and weakened calcium signaling. In the hippocampus, reversal of the reduced acetylcholine release restored calcium signaling in astrocytes, while blockade of astrocyte activation and enhancement of cholinergic innnervation repaired LTP in surgery mice. Finally, blockade of astrocyte activation improved cognitive dysfunction in surgery mice. These results provide new evidence to support that the maintenance of normal function in cholinergic inputs and astrocytes may be valuable strategies for the intervention of POD.

Neuroinflammation is considered a major contributor to POD (Lin et al., 2020; Safavynia and Goldstein, 2018). But many open questions remain at the interface between the immune system and the brain. It is well known that astrocytes play a crucial role in maintaining CNS homeostasis by cross talk with neurons and microglia (Allen and Eroglu, 2017; Kofuji and Araque, 2021). Intriguingly, in pathological conditions, the alterations in the morphology and biophysical properties of astrocytes result in a reduced capability to perform these homeostatic functions (Joe et al., 2018; Kofuji and Araque, 2021). In mice subjected to tibial fracture, we observed astrocytic gliosis in the hippocampus at early stage of POD (Fig. 2A-2C). Reactive astrogliosis induces morphological, molecular, and physiological changes (McNeill et al., 2021). Furthermore, previous studies demonstrated that electrophysiological properties of astrocytes change in response to CNS damage (Bordey et al., 2001; McNeill et al., 2021; Stephan et al., 2012). As the electrophysiological properties of astrocytes may

vary across different brain regions under physiological and disease conditions (McNeill et al., 2021), it is necessary to characterize these properties in astrocytes after major surgeries. Our data show that the physiological properties of CA1 astrocytes in surgery mice were similar to those seen in reactive astrocytes; they have depolarized resting membrane potential and higher membrane conductance and capacitance. These results suggest that the physiological functions of CA1 astrocytes are disrupted by peripheral surgery. However, further investigations are warranted to understand the mechanisms underlying the change of electrophysiological properties of astrocytes in surgery mice.

Excessive reactive astrocytes lead to numerous consequences in the function of the brain, in particular, substantially cause synaptic imbalances that induce cognitive impairment (Joe et al., 2018; Kofuji and Araque, 2021). We observed dramatic deficit in hippocampal LTP in surgery mice, which most likely resulted from impairment of glutamatergic synaptic transmission, as demonstrated by our previous study (Wang et al., 2019). Our observation that paired-pulse ratio of fEPSPs in the hippocampus were similar between sham and surgery mice, which is consistent with our previous study (Wang et al., 2019), demonstrating that impairment of glutamatergic synaptic transmission by surgery may not involve presynaptic mechanisms. We provided evidence to support that the attenuated hippocampal LTP and cognitive dysfunction in surgery mice may be associated with astrocyte activation. That is, FC, a widely used inhibitor for astrocyte activation (Hassel et al., 1992; Hennes et al., 2020), not only restored hippocampal LTP but also facilitated cognitive function in surgery mice. Interestingly, LTP in sham mice was also potentiated by FC application. These data suggest that astrocytes modulate hippocampal LTP in both naïve mice and POD mice. It has been shown that astrocytic inflammatory factors, including TNF-α, IL-1β, etc, in the hippocampus attenuate LTP induction (Butler et al., 2004; Li et al., 2016; Vereker et al., 2000). Inhibition of astrocytes with FC may lead to reduced secretion of inflammatory factors and release the inhibition of LTP in the hippocampus by these substances. Overall, our results suggest that surgery-induced cognitive impairment may originate from attenuated synaptic plasticity associated with astrocyte reactivity.

Cholinergic signaling involving neurons and non-neuronal cells participates in hippocampal synaptic transmission as well as learning and memory (Haam and Yakel, 2017; Navarrete et al., 2012; Pabst et al., 2016). In mice suffered from tibial fracture surgery, astrocyte dysfunction was accompanied by reduction of acetylcholine release

and muscarinic receptor activation in the hippocampus. It suggests that presynaptic mechanisms underlying acetylcholine release may play a significant role in cholinergic deficits following peripheral surgery.

Astrocytes in the hippocampal CA1 region are regulated by acetylcholine (Lopez-Hidalgo et al., 2012; Pabst et al., 2016) mainly through muscarinic receptors (Navarrete et al., 2012; Takata et al., 2011). In the present study, we observed that electrical stimulation evoked Ca^{2+} elevation in hippocampal astrocytes, which were mainly mediated by muscarinic receptor activation. We also observed that the surgery mice displayed compromised cholinergic transmission (Fig. 4) and concurrently reduced muscarinic receptor-mediated Ca^{2+} elevation in hippocampal astrocytes (Fig. 3), and galantamine restored electrical stimulation-evoked Ca^{2+} elevation in astrocytes in surgery mice (Fig. 5).

Although it is well established that both acetylcholine and astrocytes modulate LTP (Picciotto et al., 2012; Robert et al., 2020), it is unknown about the role that acetylcholine may play in astrocytic regulation of LTP. Our results that galantamine was sufficient to restore glutamatergic synaptic transmission (Wang et al., 2019) and LTP in the hippocampus in surgery mice (Fig. 6) support that repairing dysfunction in cholinergic signaling may be an underlying mechanism for the enhancement of glutamatergic synaptic transmission by galantamine. Astrocytes play active roles in synaptic transmission and plasticity through multiple signaling process including Ca^{2+}-dependent gliotransmission (Fiacco and McCarthy, 2018; Savtchouk and Volterra, 2018). Besides this, other structural, molecular and functional features of astrocytes contribute to astrocyte-neuronal interaction in different physiological and disease conditions (Lawal et al., 2022; Savtchouk and Volterra, 2018). Although our results about the effects of galantamine on astrocytic Ca^{2+} signaling, LTP, and synaptic transmission (Fig. 5, Fig. 6, and (Wang et al., 2019)) suggest that Ca^{2+} signaling may be involved in synaptic function in the hippocampus, further investigations are warranted to elucidate this issue.

Our pharmacological experiments used several chemicals, such as, Scop, Gal, and FC, to study mechanisms underlying dysfunction in synaptic plasticity and learning and memory in tibial fracture mice. Noteworthy is that these drugs at higher concentrations may regulate molecules other than the proposed targets. For instance, galantamine, a cholinesterase inhibitor, is an allosteric modulator of nicotinic receptors (Ago et al.,

2011); Scopolamine, a muscarinic receptor antagonist, acts as a competitive antagonist of 5-HT3 receptor (Lochner and Thompson, 2016); Fluorocitrate, a metabolic inhibitor for astrocytes, affects the synthesis of glutamine and then glutamatergic transmission (Fonnum et al., 1997; Swanson and Graham, 1994). In the present study, we chose doses of these drugs based on the literature to limit the off-target effects and cautiously drew conclusion according to these literature.

In summary, the present study shows that mice with POD exhibited multiple pathophysiological outcomes in the hippocampus, including activation and malfunction of astrocytes, reduction of acetylcholine release, impairment of muscarinic receptor function in astrocytes, and attenuated LTP in the CA1 region. These pathophysiological outcomes were reversed by restoring cholinergic inputs with galantamine and blocking astrocyte activation with fluorocitrate. These drugs improved cognitive function in POD mice. Therefore, this study provides evidence to support the notion that enhancement of cholinergic inputs to the hippocampus and blockade of astrogliosis are potential therapeutic strategies to improve cognitive function in POD.

Conflict of interest statement

The authors declare that the research was conducted without any commercial or financial conflict of interest.

Acknowledgments

This work was supported by the Natural Science Foundation of Xinjiang, China (Grant No. 2020D01C212, T.W.).

Author contribution

C.Z. and G.X. designed the experiments and supervised the study. T.W. and X.Z. performed mouse surgery. T.W., X.Z., Y.R., and T.Y. collected and analyzed image and behavioral data. C.X. and C.Z. acquired and analyzed all electrophysiological data. T.W., G.X., C.X., and C.Z. wrote the manuscript. Every author read and approved the manuscript.

References

Adam, E. H., Haas, V., Lindau, S., Zacharowski, K., Scheller, B., 2020. Cholinesterase alterations in delirium after cardiosurgery: a German monocentric prospective study. BMJ Open 10, e031212.

Ago, Y., Koda, K., Takuma, K., Matsuda, T., 2011. Pharmacological aspects of the acetylcholinesterase inhibitor galantamine. J Pharmacol Sci 116, 6-17.

Allen, N. J., Eroglu, C., 2017. Cell Biology of Astrocyte-Synapse Interactions. Neuron 96, 697-708.

Araque, A., Martin, E. D., Perea, G., Arellano, J. I., Buno, W., 2002. Synaptically released acetylcholine evokes Ca2+ elevations in astrocytes in hippocampal slices. J Neurosci 22, 2443-2450.

Bliss, T. V., Collingridge, G. L., 1993. A synaptic model of memory: long-term potentiation in the hippocampus. Nature 361, 31-39.

Boddum, K., Jensen, T. P., Magloire, V., Kristiansen, U., Rusakov, D. A., Pavlov, I., Walker, M. C., 2016. Astrocytic GABA transporter activity modulates excitatory neurotransmission. Nat Commun 7, 13572.

Bordey, A., Lyons, S. A., Hablitz, J. J., Sontheimer, H., 2001. Electrophysiological characteristics of reactive astrocytes in experimental cortical dysplasia. J Neurophysiol 85, 1719-1731.

Butler, M. P., O'Connor, J. J., Moynagh, P. N., 2004. Dissection of tumor-necrosis factor-alpha inhibition of long-term potentiation (LTP) reveals a p38 mitogen-activated protein kinase-dependent mechanism which maps to early-but not late-phase LTP. Neuroscience 124, 319-326.

Cameron, M., Kekesi, O., Morley, J. W., Tapson, J., Breen, P. P., van Schaik, A., Buskila, Y., 2016. Calcium Imaging of AM Dyes Following Prolonged Incubation in Acute Neuronal Tissue. PLoS One 11, e0155468.

Cooke, S. F., Bliss, T. V., 2006. Plasticity in the human central nervous system. Brain 129, 1659-1673.

Coyle, J., Kershaw, P., 2001. Galantamine, a cholinesterase inhibitor that allosterically modulates nicotinic receptors: effects on the course of Alzheimer's disease. Biol Psychiatry 49, 289-299.

Diaz-Castro, B., Bernstein, A. M., Coppola, G., Sofroniew, M. V., Khakh, B. S., 2021. Molecular and functional properties of cortical astrocytes during peripherally induced neuroinflammation. Cell Rep 36, 109508.

Fiacco, T. A., McCarthy, K. D., 2018. Multiple Lines of Evidence Indicate That Gliotransmission Does Not Occur under Physiological Conditions. J Neurosci 38, 3-13.

Fonnum, F., Johnsen, A., Hassel, B., 1997. Use of fluorocitrate and fluoroacetate in the study of brain metabolism. Glia 21, 106-113.

Haam, J., Yakel, J. L., 2017. Cholinergic modulation of the hippocampal region and memory function. J Neurochem 142 Suppl 2, 111-121.

Hassel, B., Paulsen, R. E., Johnsen, A., Fonnum, F., 1992. Selective inhibition of glial cell metabolism in vivo by fluorocitrate. Brain Res 576, 120-124.

Hennes, M., Lombaert, N., Wahis, J., Van den Haute, C., Holt, M. G., Arckens, L., 2020. Astrocytes shape the plastic response of adult cortical neurons to vision loss. Glia 68, 2102-2118.

Hernandez-Morales, M., Garcia-Colunga, J., 2009. Effects of nicotine on K+ currents and nicotinic receptors in astrocytes of the hippocampal CA1 region. Neuropharmacology 56, 975-983.
Hirsch, J., Vacas, S., Terrando, N., Yuan, M., Sands, L. P., Kramer, J., Bozic, K., Maze, M. M., Leung, J. M., 2016. Perioperative cerebrospinal fluid and plasma inflammatory markers after orthopedic surgery. J Neuroinflammation 13, 211.
Inouye, S. K., Westendorp, R. G., Saczynski, J. S., 2014. Delirium in elderly people. Lancet 383, 911-922.
Jing, M., Li, Y., Zeng, J., Huang, P., Skirzewski, M., Kljakic, O., Peng, W., Qian, T., Tan, K., Zou, J., Trinh, S., Wu, R., Zhang, S., Pan, S., Hires, S. A., Xu, M., Li, H., Saksida, L. M., Prado, V. F., Bussey, T. J., Prado, M. A. M., Chen, L., Cheng, H., Li, Y., 2020. An optimized acetylcholine sensor for monitoring in vivo cholinergic activity. Nat Methods 17, 1139-1146.
Jing, M., Zhang, P., Wang, G., Feng, J., Mesik, L., Zeng, J., Jiang, H., Wang, S., Looby, J. C., Guagliardo, N. A., Langma, L. W., Lu, J., Zuo, Y., Talmage, D. A., Role, L. W., Barrett, P. Q., Zhang, L. I., Luo, M., Song, Y., Zhu, J. J., Li, Y., 2018. A genetically encoded fluorescent acetylcholine indicator for in vitro and in vivo studies. Nat Biotechnol 36, 726-737.
Joe, E. H., Choi, D. J., An, J., Eun, J. H., Jou, I., Park, S., 2018. Astrocytes, Microglia, and Parkinson's Disease. Exp Neurobiol 27, 77-87.
Johansen, J. P., Cain, C. K., Ostroff, L. E., LeDoux, J. E., 2011. Molecular mechanisms of fear learning and memory. Cell 147, 509-524.
Kofuji, P., Araque, A., 2021. Astrocytes and Behavior. Annu Rev Neurosci 44, 49-67.
Lawal, O., Ulloa Severino, F. P., Eroglu, C., 2022. The role of astrocyte structural plasticity in regulating neural circuit function and behavior. Glia.
Leger, M., Quiedeville, A., Bouet, V., Haelewyn, B., Boulouard, M., Schumann-Bard, P., Freret, T., 2013. Object recognition test in mice. Nat Protoc 8, 2531-2537.
Li, D., Chen, M., Meng, T., Fei, J., 2020. Hippocampal microglial activation triggers a neurotoxic-specific astrocyte response and mediates etomidate-induced long-term synaptic inhibition. J Neuroinflammation 17, 109.
Li, W., Xu, X., Pozzo-Miller, L., 2016. Excitatory synapses are stronger in the hippocampus of Rett syndrome mice due to altered synaptic trafficking of AMPA-type glutamate receptors. Proc Natl Acad Sci U S A 113, E1575-1584.
Lin, X., Chen, Y., Zhang, P., Chen, G., Zhou, Y., Yu, X., 2020. The potential mechanism of postoperative cognitive dysfunction in older people. Exp Gerontol 130, 110791.
Lochner, M., Thompson, A. J., 2016. The muscarinic antagonists scopolamine and atropine are competitive antagonists at 5-HT3 receptors. Neuropharmacology 108, 220-228.
Lopez-Hidalgo, M., Salgado-Puga, K., Alvarado-Martinez, R., Medina, A. C., Prado-Alcala, R. A., Garcia-Colunga, J., 2012. Nicotine uses neuron-glia communication to enhance hippocampal synaptic transmission and long-term memory. PLoS One 7, e49998.
Luan, Y., Tang, D., Wu, H., Gu, W., Wu, Y., Cao, J. L., Xiao, C., Zhou, C., 2020. Reversal of hyperactive subthalamic circuits differentially mitigates pain hypersensitivity phenotypes in parkinsonian mice. Proc Natl Acad Sci U S A 117, 10045-10054.
McNeill, J., Rudyk, C., Hildebrand, M. E., Salmaso, N., 2021. Ion Channels and Electrophysiological Properties of Astrocytes: Implications for Emergent Stimulation Technologies. Front Cell Neurosci 15, 644126.
Moskowitz, E. E., Overbey, D. M., Jones, T. S., Jones, E. L., Arcomano, T. R., Moore, J. T.,

Robinson, T. N., 2017. Post-operative delirium is associated with increased 5-year mortality. Am J Surg 214, 1036-1038.
Navarrete, M., Perea, G., Fernandez de Sevilla, D., Gomez-Gonzalo, M., Nunez, A., Martin, E. D., Araque, A., 2012. Astrocytes mediate in vivo cholinergic-induced synaptic plasticity. PLoS Biol 10, e1001259.
Ota, Y., Zanetti, A. T., Hallock, R. M., 2013. The role of astrocytes in the regulation of synaptic plasticity and memory formation. Neural Plast 2013, 185463.
Pabst, M., Braganza, O., Dannenberg, H., Hu, W., Pothmann, L., Rosen, J., Mody, I., van Loo, K., Deisseroth, K., Becker, A. J., Schoch, S., Beck, H., 2016. Astrocyte Intermediaries of Septal Cholinergic Modulation in the Hippocampus. Neuron 90, 853-865.
Pandharipande, P. P., Girard, T. D., Jackson, J. C., Morandi, A., Thompson, J. L., Pun, B. T., Brummel, N. E., Hughes, C. G., Vasilevskis, E. E., Shintani, A. K., Moons, K. G., Geevarghese, S. K., Canonico, A., Hopkins, R. O., Bernard, G. R., Dittus, R. S., Ely, E. W., Investigators, B.-I. S., 2013. Long-term cognitive impairment after critical illness. N Engl J Med 369, 1306-1316.
Picciotto, M. R., Higley, M. J., Mineur, Y. S., 2012. Acetylcholine as a neuromodulator: cholinergic signaling shapes nervous system function and behavior. Neuron 76, 116-129.
Popov, A., Brazhe, A., Denisov, P., Sutyagina, O., Li, L., Lazareva, N., Verkhratsky, A., Semyanov, A., 2021. Astrocyte dystrophy in ageing brain parallels impaired synaptic plasticity. Aging Cell 20, e13334.
Popov, A., Denisov, P., Bychkov, M., Brazhe, A., Lyukmanova, E., Shenkarev, Z., Lazareva, N., Verkhratsky, A., Semyanov, A., 2020. Caloric restriction triggers morphofunctional remodeling of astrocytes and enhances synaptic plasticity in the mouse hippocampus. Cell Death Dis 11, 208.
Reeves, A. M., Shigetomi, E., Khakh, B. S., 2011. Bulk loading of calcium indicator dyes to study astrocyte physiology: key limitations and improvements using morphological maps. J Neurosci 31, 9353-9358.
Robert, V., Therreau, L., Davatolhagh, M. F., Bernardo-Garcia, F. J., Clements, K. N., Chevaleyre, V., Piskorowski, R. A., 2020. The mechanisms shaping CA2 pyramidal neuron action potential bursting induced by muscarinic acetylcholine receptor activation. J Gen Physiol 152.
Saczynski, J. S., Marcantonio, E. R., Quach, L., Fong, T. G., Gross, A., Inouye, S. K., Jones, R. N., 2012. Cognitive trajectories after postoperative delirium. N Engl J Med 367, 30-39.
Safavynia, S. A., Goldstein, P. A., 2018. The Role of Neuroinflammation in Postoperative Cognitive Dysfunction: Moving From Hypothesis to Treatment. Front Psychiatry 9, 752.
Savtchouk, I., Volterra, A., 2018. Gliotransmission: Beyond Black-and-White. J Neurosci 38, 14-25.
Schenning, K. J., Murchison, C. F., Mattek, N. C., Kaye, J. A., Quinn, J. F., 2019. Sex and genetic differences in postoperative cognitive dysfunction: a longitudinal cohort analysis. Biol Sex Differ 10, 14.
Shi, X. D., Sun, K., Hu, R., Liu, X. Y., Hu, Q. M., Sun, X. Y., Yao, B., Sun, N., Hao, J. R., Wei, P., Han, Y., Gao, C., 2016. Blocking the Interaction between EphB2 and ADDLs by a Small Peptide Rescues Impaired Synaptic Plasticity and Memory Deficits in a Mouse Model of Alzheimer's Disease. J Neurosci 36, 11959-11973.
Skvarc, D. R., Berk, M., Byrne, L. K., Dean, O. M., Dodd, S., Lewis, M., Marriott, A., Moore, E. M., Morris, G., Page, R. S., Gray, L., 2018. Post-Operative Cognitive Dysfunction: An

exploration of the inflammatory hypothesis and novel therapies. Neurosci Biobehav Rev 84, 116-133.
Solari, N., Hangya, B., 2018. Cholinergic modulation of spatial learning, memory and navigation. Eur J Neurosci 48, 2199-2230.
Stephan, J., Haack, N., Kafitz, K. W., Durry, S., Koch, D., Hochstrate, P., Seifert, G., Steinhauser, C., Rose, C. R., 2012. Kir4.1 channels mediate a depolarization of hippocampal astrocytes under hyperammonemic conditions in situ. Glia 60, 965-978.
Swanson, R. A., Graham, S. H., 1994. Fluorocitrate and fluoroacetate effects on astrocyte metabolism in vitro. Brain Res 664, 94-100.
Takata, N., Mishima, T., Hisatsune, C., Nagai, T., Ebisui, E., Mikoshiba, K., Hirase, H., 2011. Astrocyte calcium signaling transforms cholinergic modulation to cortical plasticity in vivo. J Neurosci 31, 18155-18165.
Tang, D. L., Luan, Y. W., Zhou, C. Y., Xiao, C., 2021. D2 receptor activation relieves pain hypersensitivity by inhibiting superficial dorsal horn neurons in parkinsonian mice. Acta Pharmacol Sin 42, 189-198.
Terrando, N., Eriksson, L. I., Ryu, J. K., Yang, T., Monaco, C., Feldmann, M., Jonsson Fagerlund, M., Charo, I. F., Akassoglou, K., Maze, M., 2011. Resolving postoperative neuroinflammation and cognitive decline. Ann Neurol 70, 986-995.
Terrando, N., Gomez-Galan, M., Yang, T., Carlstrom, M., Gustavsson, D., Harding, R. E., Lindskog, M., Eriksson, L. I., 2013. Aspirin-triggered resolvin D1 prevents surgery-induced cognitive decline. FASEB J 27, 3564-3571.
Vereker, E., O'Donnell, E., Lynch, M. A., 2000. The inhibitory effect of interleukin-1beta on long-term potentiation is coupled with increased activity of stress-activated protein kinases. J Neurosci 20, 6811-6819.
Wang, T., Zhu, H., Hou, Y., Gu, W., Wu, H., Luan, Y., Xiao, C., Zhou, C., 2019. Galantamine reversed early postoperative cognitive deficit via alleviating inflammation and enhancing synaptic transmission in mouse hippocampus. Eur J Pharmacol 846, 63-72.
Wilson, J. E., Mart, M. F., Cunningham, C., Shehabi, Y., Girard, T. D., MacLullich, A. M. J., Slooter, A. J. C., Ely, E. W., 2020. Delirium. Nat Rev Dis Primers 6, 90.
Xiong, C., Zhang, Z., Baht, G. S., Terrando, N., 2018. A Mouse Model of Orthopedic Surgery to Study Postoperative Cognitive Dysfunction and Tissue Regeneration. J Vis Exp.
Zhang, X., Yao, H., Qian, Q., Li, N., Jin, W., Qian, Y., 2016. Cerebral Mast Cells Participate In Postoperative Cognitive Dysfunction by Promoting Astrocyte Activation. Cell Physiol Biochem 40, 104-116.
Zhao, B., Ni, Y., Tian, X., 2019. Low Plasma Cholinesterase Activity is Associated With Postoperative Delirium After Noncardiac Surgery in Elderly Patients: AProspective Observational Study. Psychosomatics 60, 190-196.

Figure legends

Figure 1 Surgery mice exhibit memory impairment.

(A) Schematic diagram showing a context dependent fear-conditioning protocol for **(B)** – **(D)** (see Methods and Materials). Conditioning and testing sessions were respectively performed 1 day before (Day -1) and 3 days after (Day 3) sham or surgery. **(B - C)** Freezing behavior of sham and surgery mice during baseline (pre-conditioning) and three trials of fear conditioning. **(B)** $t = 0.89$, $P = 0.39$, $n = 8$ in each group. **(C)** Group, $F_{(1, 14)} = 2.12$, $P = 0.17$; Trial, $F_{(3, 42)} = 150.3$, $P < 0.0001$; Interaction, $F_{(3, 42)} = 1.17$, $P = 0.33$, $n = 8$ in each group. **(D)** Freezing behavior during testing session. $t = 5.01$, $P = 0.0002$, $n = 8$ in each group. **(E)** Schematic diagram showing a protocol for novel object recognition test (NOR) in **(F–I)**. **(F)** Examples of movement tracks of sham and surgery mice in the test arena during testing session. **(G-H)** The total time that sham and surgery mice spent exploring objects during 10 min training session (**G**, $F_{(3, 38)} = 0.76$, $P = 0.52$) and testing session (**H**, $F_{(3, 38)} = 5.31$, $P = 0.004$). **(I)** The ratio of time spent in exploring the novel object to total time spent exploring the novel and familiar objects. $t = 3.3$, $P = 0.004$. $n = 10$ in sham group, $n = 11$ in surgery group in **(E)**–**(I)**. ** $P < 0.01$, Unpaired t-test in **(B)**, **(D)** and **(I)**; Two way ANOVA with Bonferroni post-hoc analysis in **(C)**; One way ANOVA with Bonferroni post-hoc analysis in **(G)**, **(H)**.

Figure 2 Surgery leads to activation and biophysical modification of astrocytes in the hippocampus.

(A) Representative images showing GFAP-staining of the hippocampal CA1 Stratum Radiatum from sham and surgery mice 3 days after operation. **(B)** Quantification of the density of GFAP-positive astrocytes measured in 100 × 100 μm^2 area from sham and surgery mice. t = 3.05, P = 0.0087, n = 8 mice in each group. **(C)** Relative total GFAP-immunoreactive area in the hippocampal CA1 region, normalized to the average of the area in sham mice. t = 4.31, P = 0.0005, surgery vs. sham, n = 9 mice in each group. ** P < 0.01, unpaired t-test was used in **(B)** and **(C)**. **(D)** Upper panel: diagram showing recording of astrocytes in the alveus of the hippocampal CA1 region. Lower panel: Example image of a patch-clamp recorded astrocyte labeled with sulforhodamine 101 (SR101) in the alveus. **(E)** Recordings of currents in response to voltage steps from -100 mV to +40 mV with a 10 mV increment delivered through the patch pipette to voltage-clamped astrocytes (held at -80 mV) from sham and surgery mice. **(F)** Current-voltage (I-V) relationships in hippocampal astrocytes in sham and surgery mice. Sham vs surgery: $F_{(1, 13)} = 5.84$, P = 0.031; Voltage step: $F_{(14, 182)} = 356.9$, P < 0.0001; Interaction: $F_{(14, 182)} = 1.47$, P < 0.0001. **(G - I)** Quantification of the resting membrane potential (Vm) (**G**, t = 0.38, P = 0.004, n = 10 from 4 mice in each group), conductance (**H**, t = 2.48, P = 0.02, n = 10 from 4 mice in each group), and capacitance of hippocampal astrocytes from sham and surgery mice (**I**, t = 2.60, P = 0.017, n = 10 from 4 mice in each group). Unpaired t-test in **(G-I)**, two way ANOVA with Bonferroni post-hoc analysis in **(F)**.

Figure 3 Surgery impairs electrically evoked calcium elevation in hippocampal astrocytes.

(A) Example images of astrocytes labeled with SR101 and filled with Fluo-4, a calcium indicator. Arrows indicate astrocytes co-labeled with SR101 and Fluo-4. **(B)** Schematic diagram showing electrical stimulation of the Stratum oriens / alveus (O/A) in the hippocampal CA1 region used for Ca^{2+} imaging in astrocytes. **(C)** Pseudocolor images of fluorescence intensity of Fluo-4 in astrocytes before, during and after O/A stimulation. **(D)** Electrical stimulation evoked an enhancement of Fluo-4 fluorescence in astrocytes. **(E)** Percentage of astrocytes responded to electrical stimulation in sham and surgery mice. 54.8% ± 2.35%, n = 8 regions from 5 sham mice; 52.9% ± 6.36%, n = 6 regions from 5 surgery mice, t = 0.32, P = 0.75. **(F)** Quantification of electrical stimulation-evoked peak responses in astrocytes. t = 4.58, P < 0.0001, n = 23 cells from 5 sham mice, n = 18 cells from 5 surgery mice. **(G - J)** Normalized average traces (**G** and **I**) and peak responses (**H** and **J**) of Fluo-4 fluorescence in hippocampal astrocytes from sham and surgery mice evoked by O/A stimulation in control and presence of scopolamine (Scop, 5 μM). **(H)** sham: t = 6.6, P < 0.0001, n = 10. **(J)** surgery: t = 5.74, P < 0.0001, n = 11. **(K)** Electrical stimulation-evoked Scop-sensitive component of Fluo-4 responses. **(L)** Quantification of Scop-sensitive components of stimulation-evoked Fluo-4 peak responses. t = 3.37, P = 0.003, n = 10 in sham group, n = 11 in surgery group. ** P < 0.01, Two-tailed unpaired t-test in **(E)**, **(F)**, **(H)**, **(J)** and **(L)**.

Figure 4 Surgery impairs acetylcholine release in the hippocampus.

(A) AAV-hSyn-GACh3.0 was injected in the hippocampus. Upper panel, the diagram of viral injection and a typical image showing efficient transfection of the GACh vector in the hippocampus. Lower panel, electrical stimulation was applied to evoke acetylcholine (ACh) release. **(B)** Pseudocolor images showing GACh fluorescence signal recorded before, during, and after electrical stimulation. **(C-D)** Averaged normalized traces **(C)** and summary **(D)** of peak responses in sham and surgery mice. **(D)** $t = 2.87$, $P = 0.008$, $n = 15$ from 5 sham mice, $n = 15$ from 5 surgery mice, unpaired two-tailed t-test. Dashed vertical line in **(C)** indicates the time point of O/A stimulation.

Figure 5 Accumulation of ACh enhances electrical stimulation-evoked calcium elevation in hippocampal astrocytes.

Example traces (**A** and **C**) and quantification (**B** and **D**) of O/A stimulation-evoked changes in Fluo-4 signals in hippocampal astrocytes from sham and surgery mice in the absence and presence of galantamine (Gal, 5 μM). Dashed line indicates electrical stimulation of the O/A area of the hippocampal CA1 region. **(B)** $t = 6.51$, $P < 0.0001$, $n = 11$ regions from 5 sham mice, two-tailed paired t-test. **(D)** $t = 10.76$, $P < 0.0001$, $n = 12$ regions from 5 surgery mice, two-tailed paired t-test. **(E)** Electrical stimulation-induced enhancement of Fluo-4 signal. 28.07% ± 4.72%, $n = 11$ regions from 5 sham mice; 61.21% ± 6.21%, $n = 12$ regions from 5 surgery mice. $t = 4.19$, $P = 0.0004$, sham vs. surgery, unpaired two-tailed t-test.

Figure 6 Fluorocitrate and galantamine restore synaptic plasticity in the hippocampus of surgery mice.

(A) Example image showing the stimulating electrode in the Schaffer collaterals (SC) and the recording electrode in CA1 in hippocampal slice (upper panel). Schematic diagram showing high frequency stimulation (HFS) protocol for recording fEPSPs in hippocampal CA1 region (lower panel). **(B)** Example traces of fEPSPs before and 40 min after HFS (see Methods and Materials). **(C)** Time courses of fEPSP amplitude before and after HFS in hippocampal slices from sham and surgery mice. fEPSP amplitude is normalized to the mean of fEPSP amplitude prior to HFS. **(D)** Summary of LTP amplitude 40 - 60 min after stimulation. t = 4.48, P = 0.0003, n = 10 slices from 5 mice in each group. **(E)** Example traces of fEPSPs evoked by paired-pulse stimulation (100 ms interval) before and 40 min after HFS. **(F)** The paired-pulse ratio (PPR) before and 40 min after HFS in sham and surgery mice. Group: $F_{(1, 32)}$ = 10.09, P = 0.0033; Baseline vs post-HFS: $F_{(1, 32)}$ = 0.10, P = 0.75; Interaction: $F_{(1, 32)}$ = 0.0011, P = 0.97; n = 9 slices from 5 mice in each group. **(G)** Example traces of fEPSPs before and 40 min after HFS from hippocampal slices without (ACSF) and with treatment of FC (100 μM, an inhibitor of astrocyte activation) or Gal (10 μM) from sham mice. **(H)** fEPSP amplitudes relative to the baseline levels versus time in control (ACSF) and in the presence of fluorocitrate (FC) or galantamine (Gal) in hippocampal slices from sham mice. **(I)** Summary of LTP amplitudes 40 - 60 min after HFS in normal ACSF (ACSF, n = 10) and in the presence of FC (n = 6) or Gal (n = 6). $F_{(2, 19)}$ = 11.1, P = 0.0006. **(J)** Example traces of fEPSPs in hippocampal slices from surgery mice before and 40 min after HFS without (ACSF) and with treatment of FC (100 μM) or Gal (10 μM). **(K)** fEPSP amplitudes relative to baseline level versus time in ACSF and in the presence of FC or Gal in surgery hippocampal slices. **(L)** Summary of LTP amplitudes 40 - 60 min after HFS in control (n = 10), FC (n = 6), and Gal (n = 5) in surgery hippocampal slices. $F_{(2, 18)}$ = 26.99, P < 0.0001. Unpaired t-test used in **(D)**, two-way ANOVA with Bonferroni post-hoc analysis in **(F),** one way ANOVA with Bonferroni post-hoc analysis in **(I)** and **(L)**.

Figure 7 Intra-hippocampal injection of fluorocitrate facilitated learning and memory in surgery mice

(A) Schematic diagram of cannula implantation and drug injection in the hippocampus of surgery mice. **(B)** Left panel, a representative brain section showing cannula placement above the dorsal hippocampus. Right panel, locations of the tips of the cannulas in all surgery mice. Each red circle represents the location of a cannula. **(C)** Representative images showing that FC local injection for 3 days reduced astrocyte activation. Green, GFAP-immunoreactive. Scale bar: 50 μm. **(D)** GFAP-positive cells were counted and GFAP-positive areas were measured in each images acquired under a 20× objective. A total of 15 images from 5 mice, 3 from each, were included. Left panel: $t = 7.237$, $df = 28$, $P < 0.0001$, sham vs. surgery. Right panel: $t = 5.607$ $df = 28$, $P < 0.0001$, sham vs. surgery. **(E-F)** Fear-conditioning test were performed in surgery mice received 3 day saline or fluorocitrate (FC) injection in the hippocampus. Freezing behaviors in pre-conditioning and testing sessions were summarized. **(E)** Pre-conditioning, $t = 0.33$, $P = 0.75$; $n = 8$ in each group. **(F)** Testing session, $t = 2.66$, $P = 0.018$, $n = 8$ in each group. **(G)** The total time that saline and FC mice spent exploring objects during 10 min training session (Saline: $t = 1.02$, $P = 0.32$; FC: $t = 0.49$, $P = 0.63$; $n = 8$ in saline group, $n = 7$ in FC group) **(H)** Examples of movement tracks in the test arena during testing session. **(I)** The total time that saline and FC mice spent exploring objects during testing session. Saline: $t = 0.005$, $P = 1.0$; FC: $t = 2.62$, $P = 0.02$; $n = 8$ in saline group, $n = 7$ in FC group. **(J)** Novel object discrimination index in saline and FC surgery mice. $t = 2.87$, $P = 0.013$; $n = 8$ in saline group, $n = 7$ in FC group. * $P < 0.05$, two-tailed, unpaired t-test in **(D-G)**, **(I)** and **(J)**.

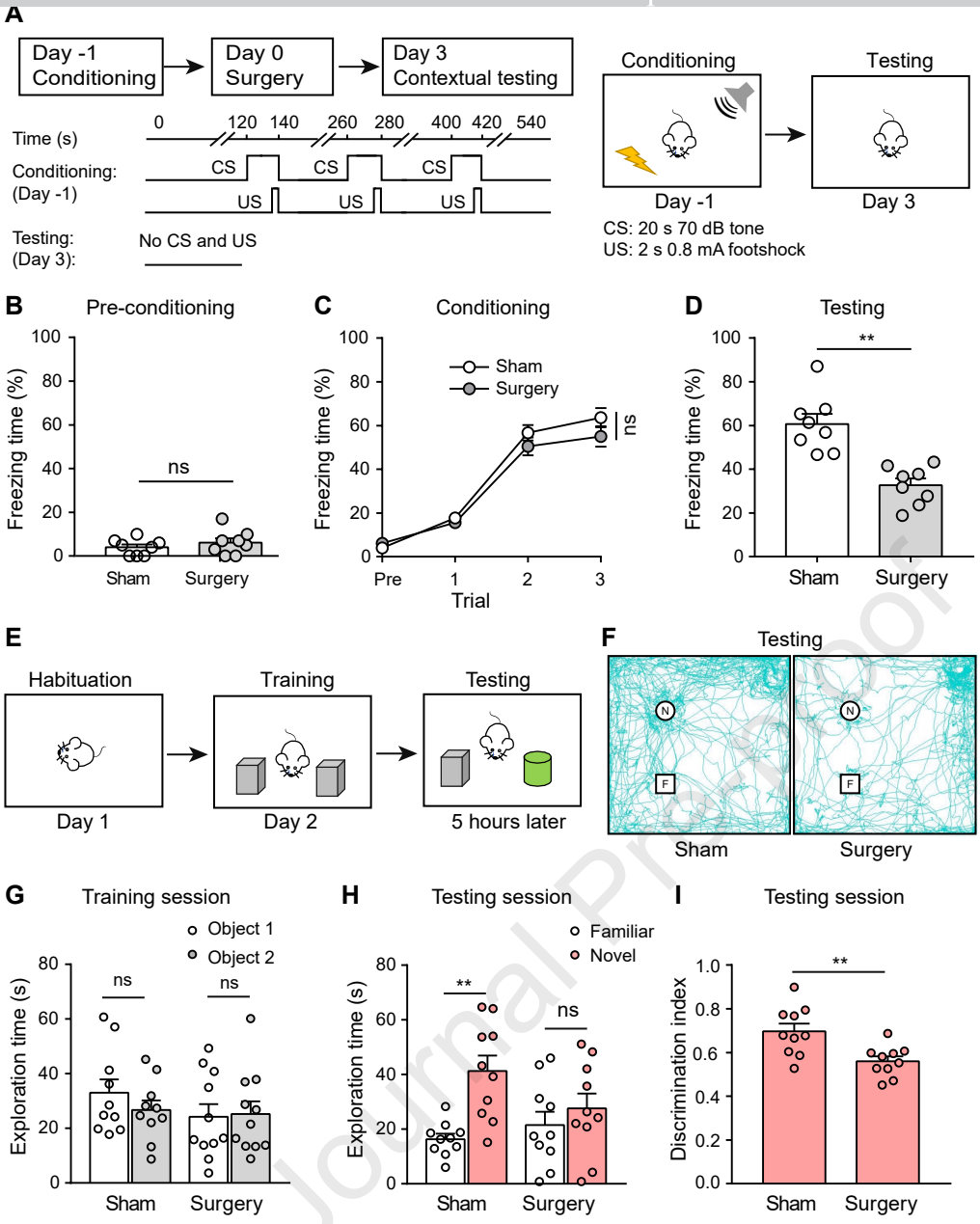

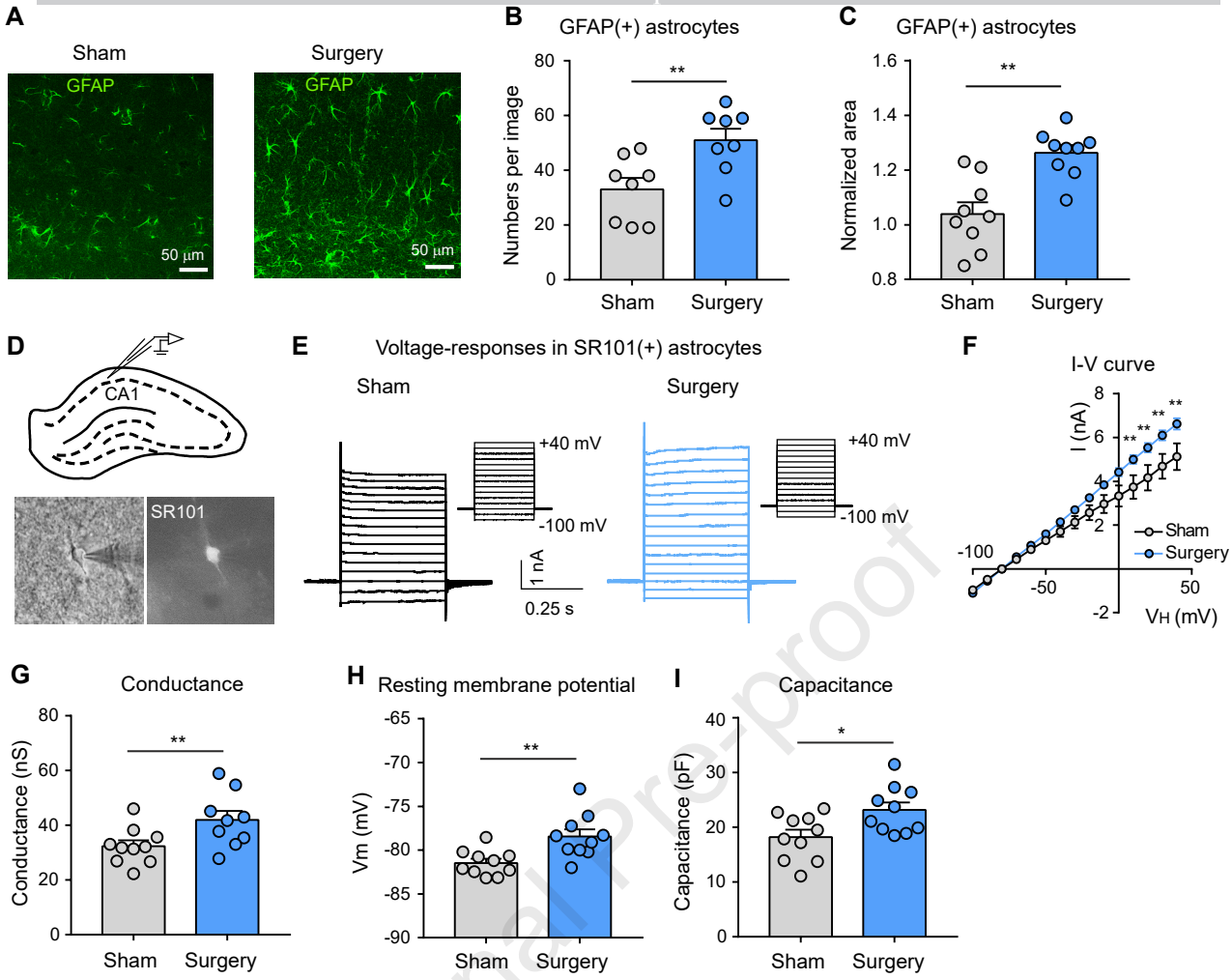

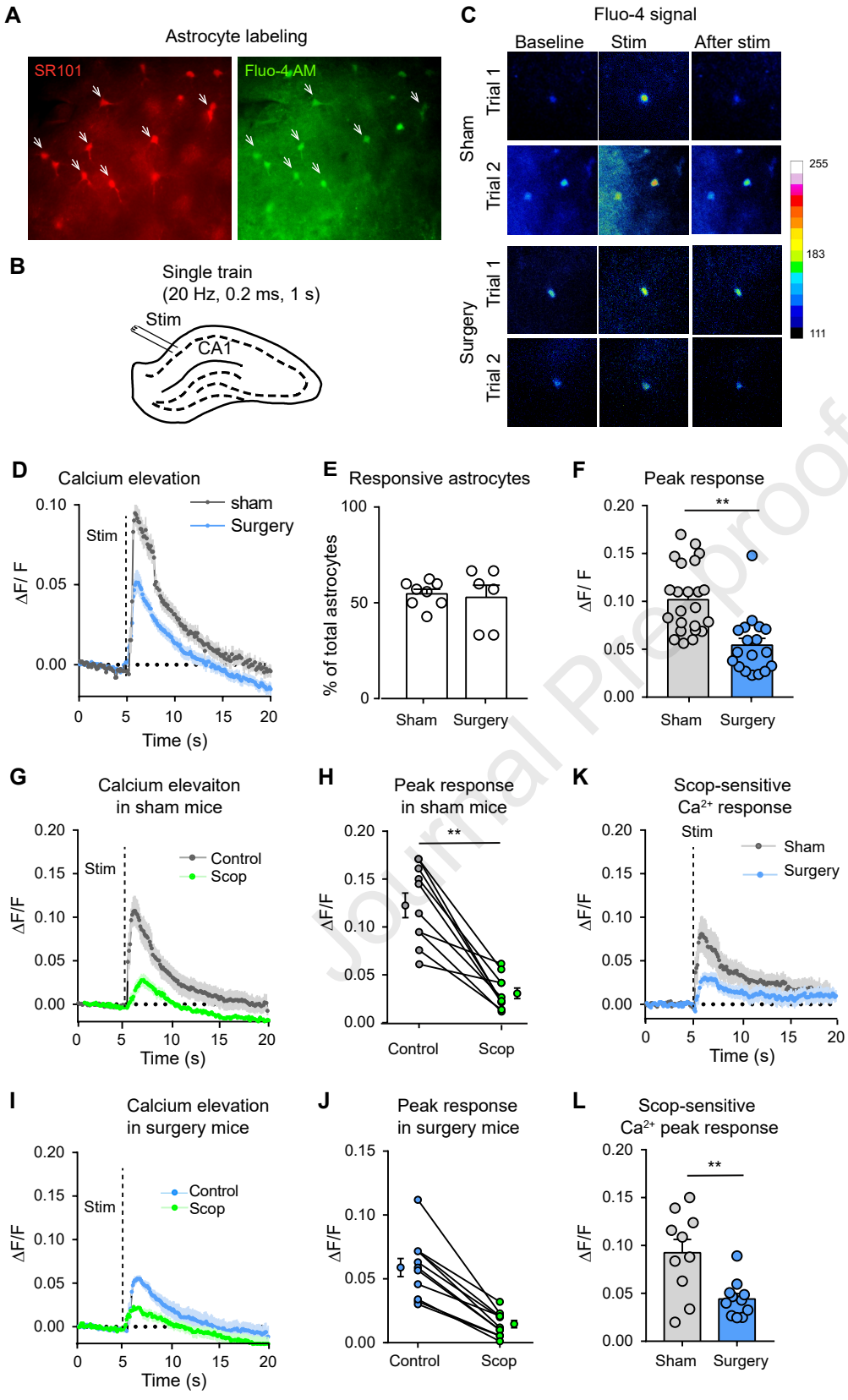

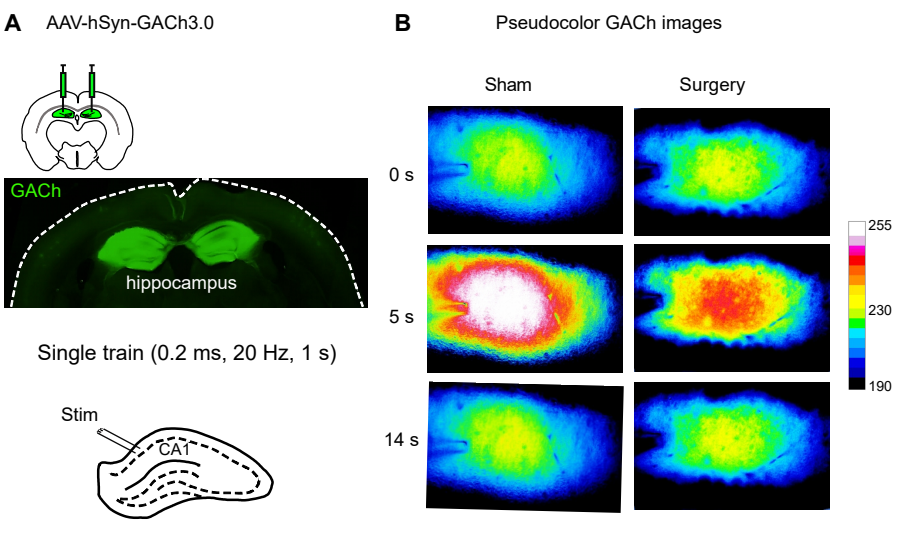

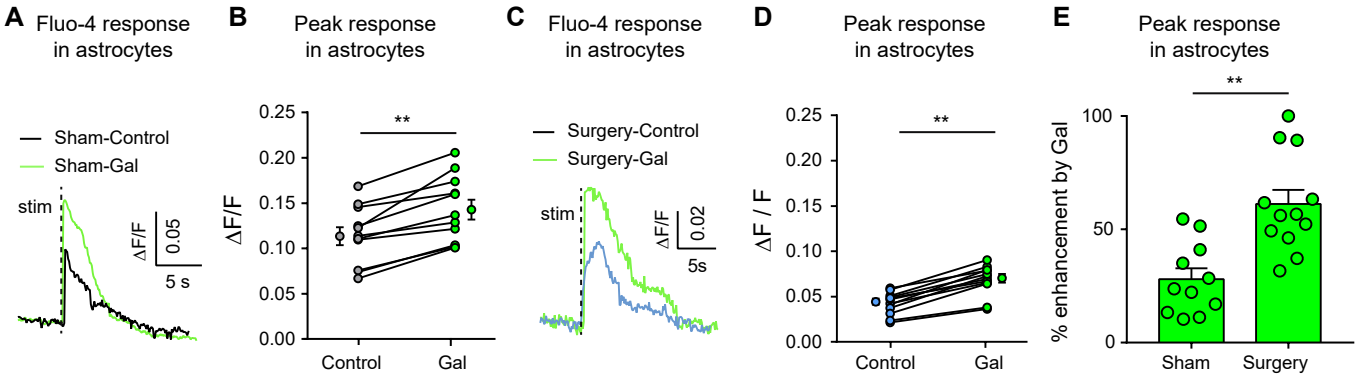

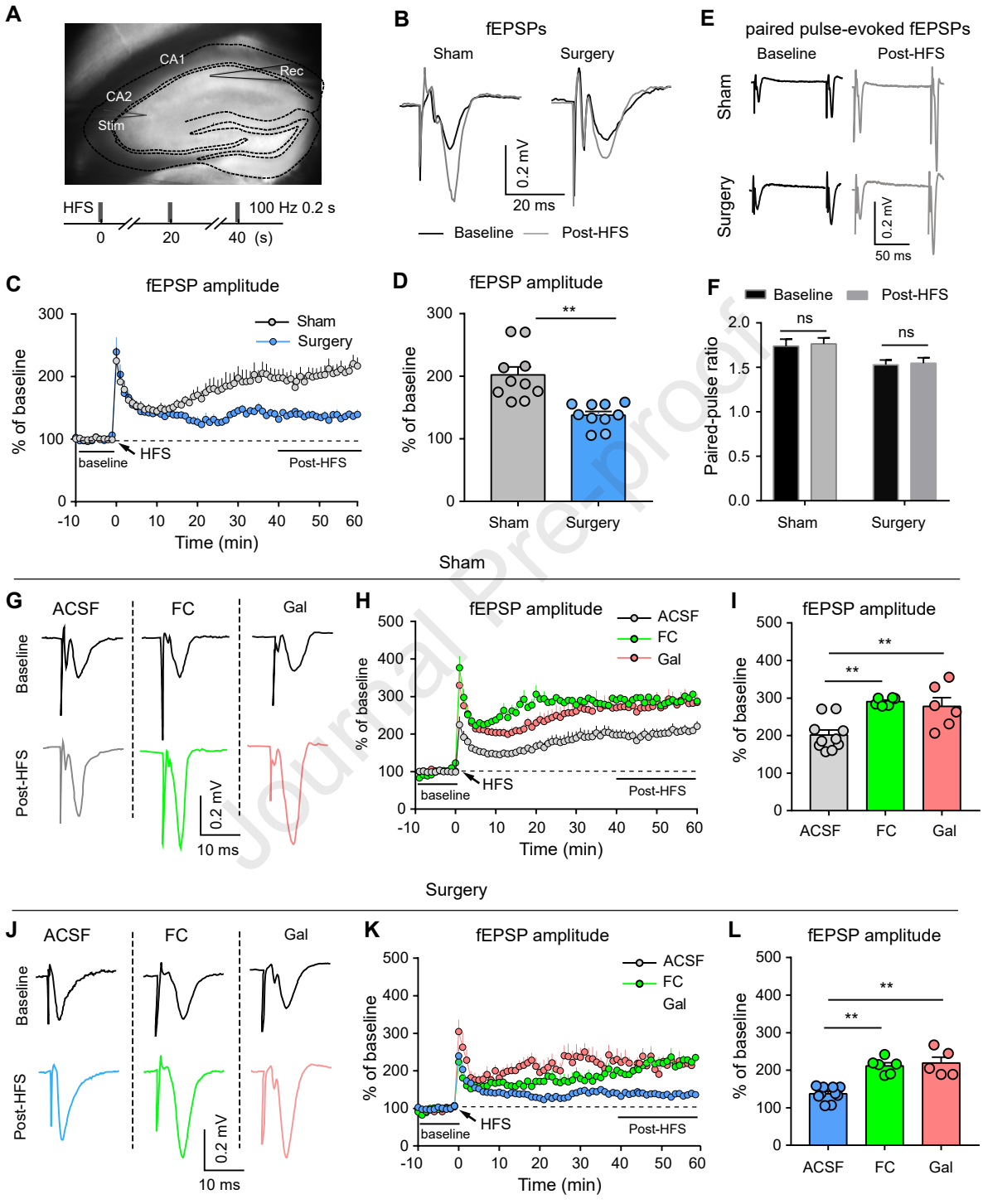
A
CA1
CA2
Rec
Stim
HFS
100 Hz 0.2 s
0
20
40 (s)
B
fEPSPs
Sham
Surgery
0.2 mV
20 ms
Baseline
Post-HFS
E
paired pulse-evoked fEPSPs
Baseline
Post-HFS
Sham
Surgery
0.2 mV
50 ms
C
fEPSP amplitude
Sham
Surgery
% of baseline
baseline
HFS
Post-HFS
Time (min)
D
fEPSP amplitude
**
% of baseline
Sham
Surgery
F
Baseline
Post-HFS
ns
ns
Paired-pulse ratio
Sham
Surgery
Sham
G
ACSF
FC
Gal
Baseline
Post-HFS
0.2 mV
10 ms
H
fEPSP amplitude
ACSF
FC
Gal
% of baseline
baseline
HFS
Post-HFS
Time (min)
I
fEPSP amplitude
**
**
% of baseline
ACSF
FC
Gal
Surgery
J
ACSF
FC
Gal
Baseline
Post-HFS
0.2 mV
10 ms
K
fEPSP amplitude
ACSF
FC
Gal
% of baseline
baseline
HFS
Post-HFS
Time (min)
L
fEPSP amplitude
**
**
% of baseline
ACSF
FC
Gal

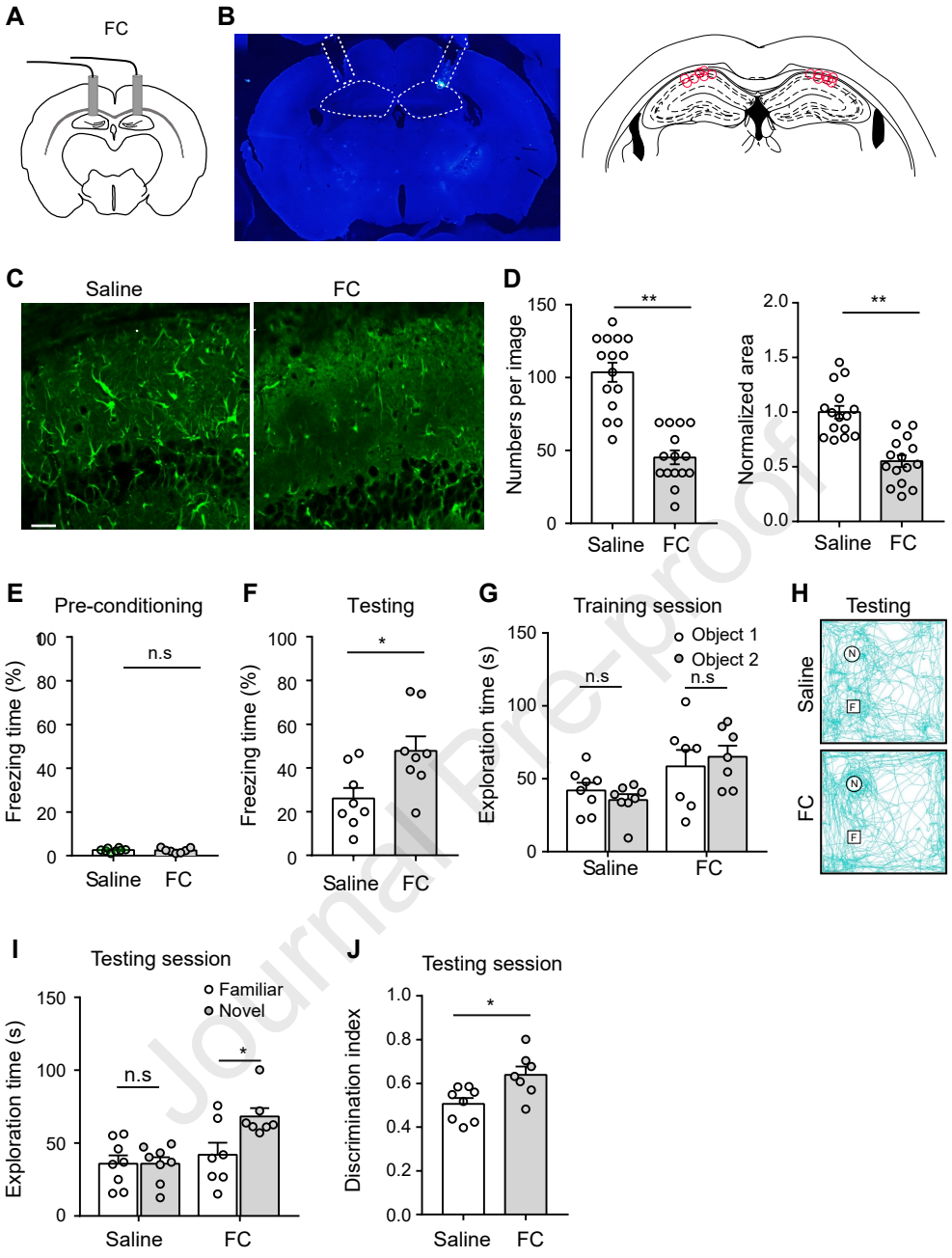

Highlights:

- Peripheral surgery attenuates acetylcholine release, activates astrocytes, restrains acetylcholine-evoked calcium signaling in astrocytes, and impairs LTP in the hippocampus.
- The restrained calcium signaling in the astrocytes is restored by correcting the diminution of acetylcholine release in the hippocampus of surgery mice.
- Blocking astrocyte activation normalized hippocampal LTP and cognitive function in surgery mice.
- The maintenance of normal function in astrocytes and cholinergic inputs may be valuable strategies for the intervention of cognitive dysfunction in postoperative delirium.